Key Engineering Materials
ISSN: 1662-9795, Vol. 926, pp 1039-1050
doi:10.4028/p-w5x675

Submitted: 2021-12-08
Revised: 2022-01-25
Accepted: 2022-02-04
Online: 2022-07-22

A Novel Method for the Determination of High Temperature FLCs of ECAP-Processed Aluminum AA5083 Sheet Metal

Maximilian Gruber[1,a*], Philipp Leitner[1,b], Matthias Auer[1,c], Christian Illgen[2,d], Philipp Frint[2,e], Martin F.-X. Wagner[2,f] and Wolfram Volk[1,g]

[1]Chair of Metal Forming and Casting, Technical University of Munich, Walther-Meissner-Str. 4, Garching 85748, Germany

[2]Institute of Materials Science and Engineering, Chemnitz University of Technology, Erfenschlager Str. 73, Chemnitz 09125, Germany

[a]maximilian.gruber@utg.de; [b]philipp.leitner@tum.de; [c]matthias.auer@tum.de; [d]christian.illgen@mb.tu-chemnitz.de; [e]philipp.frint@mb.tu-chemnitz.de; [f]martin.wagner@mb.tu-chemnitz.de; [g]wolfram.volk@utg.de

Keywords: Equal-channel angular pressing (ECAP), Aluminum AA5083, hot Forming Limit Curve (FLC)

Abstract. In this study, investigations into the deformation behavior of aluminum AA5083 at elevated temperatures were carried out on a newly developed test rig. The test rig was developed jointly with ZwickRoell GmbH & Co. KG (Germany) and is based on a Nakajima test carried out with heated dies. In this way, statements can be made about the lightweight potential of the alloy. Additionally, equal-channel angular pressing (ECAP) was performed to process the aluminum sheet metal. The conventional ECAP process is mainly used for bulk material in laboratory use and therefore is often not suitable for industrial applications, especially for large series. The use of sheet metal allows a significant increase in the areas of application. It is documented in conventional ECAP that grain refinement is achieved by the severe plastic deformation. At room temperature this primarily increases the mechanical strength. Formability is improved in fine-grained materials, especially at elevated temperatures, which is related to diffusion-controlled deformation mechanisms and grain boundary sliding. The advantages of ECAP for sheet materials are thus also in lightweight construction and can expand the scope of application of the AA5083 alloy. ECAP-route C was used for the process to provide the most homogeneous microstructure possible (180° rotation around the ECAP-axis after the first pass). Nakajima specimens were taken from the processed sheet materials to determine the Forming Limit Curve (FLC) compared to the reference material (four different specimen geometries). FLCs under elevated temperatures (250 °C, 375 °C) were determined on the novel Nakajima test bench. A special feature of the test rig is the rapid heating to avoid microstructural changes. Microscopic examinations were performed after the deformation to study the deformation mechanisms. Differences of the forming and fracture mechanisms between the reference alloy and the ECAP material were found.

Introduction

Aluminum as a lightweight material is playing an increasingly important role in the automotive sector. A weight reduction of up to 40 % can be achieved when compared to steel. As a result, vehicle bodies can be built significantly lighter and fuel or electrical consumption is reduced. This topic has received a great deal of attention since 2014, when it became mandatory for the automotive industry to reduce CO_2 emissions from the current level of around 140 g/km to 95 g/km in the European Union by 2021. While approximately 150 kg of aluminum is now used per passenger car, this figure is set to grow to almost 200 kg by 2025. The automotive sector is therefore seen as having the greatest development potential in terms of materials requirements and technologies [1,2].

Other elements are usually added to aluminum to deliberately change its properties. AlMg(Mn) alloys, for example, are characterized by medium to high static strength and good fatigue properties. In addition, they have high cold formability, corrosion resistance, and good weldability, provided the

Mg content is above 3 wt.-% [1]. Despite many advantages, these alloys, which belong to the 5000 series, also exhibit disadvantages. These include, above all, limited formabilty and significant springback [3]. For these reasons, AlMg(Mn) alloys are less likely to be processed into structural profiles, but rather into rolled products [1]. The disadvantages can be eliminated, for example, if the forming process is carried out at elevated temperatures. This results in the following potentials [4]:

- Shifting of the forming limits
- Reduction of forming forces and pressures
- Improved component accuracy

One special approach to achieve very high formability is superplastic forming (SPF). In principle, SPF can produce very complex component geometries, which is why this process becomes increasingly important in the interest of lightweight construction [5]. The following process requirements must be met to obtain superplasticity [6,7]: Forming temperature above the recrystallization temperature and very low forming rates (10^{-5} 1/s < $\dot{\varphi}$ < 10^{-3} 1/s). In addition, superplastic materials must fulfill certain material-technical prerequisites [5]: Isotropic material structure, globular grains and a fine-grained microstructure (grain diameter < 10 µm). This microstructure can be achieved, for example, with Severe Plastic Deformation (SPD) processes such as equal-channel angular pressing (ECAP) [8]. ECAP is predominantly used on a laboratory scale and for bulk materials [9]. In order to apply the advantages of this process in automotive and large-series industrial manufacturing, ECAP was further developed for sheet materials [10,11]. However, the material- and process-related forming temperatures must be precisely matched in order to make the best possible use of these potentials. This is where the objective of this paper comes in, by investigating the formability of AA5083 aluminum sheets at various elevated temperatures.

Equal-Channel Angular Pressing for Aluminum Sheet Metal

The following section describes the ECAP tests. Sheets of aluminum alloy AA5083 were used for all tests. The dimensions of the rolled sheets were 200 mm x 200 mm x 1.8 mm and they were annealed at 500 °C for one hour before processing to provide a homogeneous microstructure. In the ECAP process, the sheets were pressed through the angled die at a punch speed of 5 mm/s at room temperature (RT). The tool is composed of left and right channel parts, see Figure 1. The channel forms an ECAP angle of 120° and the channel parts each have a radius (inner and outer, respectively) of 0.5 mm. The channel width w_{N1} was 2.05 mm for the first pass (N1), and the channel height h_{N1} was 1.85 mm. After the first pass, the specimens were rotated by 180° in the ECAP direction (ED) to perform route C. A channel width, $w_{C2,}$ of 2.25 mm and a height, $h_{C2,}$ of 1.85 mm were chosen for the second pass. Bechem Beruforge 150D lubricant was used to reduce friction [12,13]. According to Iwahashi's formula, equivalent plastic strains of 0.67 can be obtained for the first pass and also in the second pass, when the material is fully pressed into the outer radius ($\Phi = 120°$, $\psi = 0°$) [14]. However, since no back pressure was used for the tests, the material did not completely fill the outer radius and therefore an outer angle of $\psi = 60°$ was assumed. This results in an equivalent plastic strain of 0.6 for the passes, which corresponds to a total equivalent plastic of 1.2 according to route C.

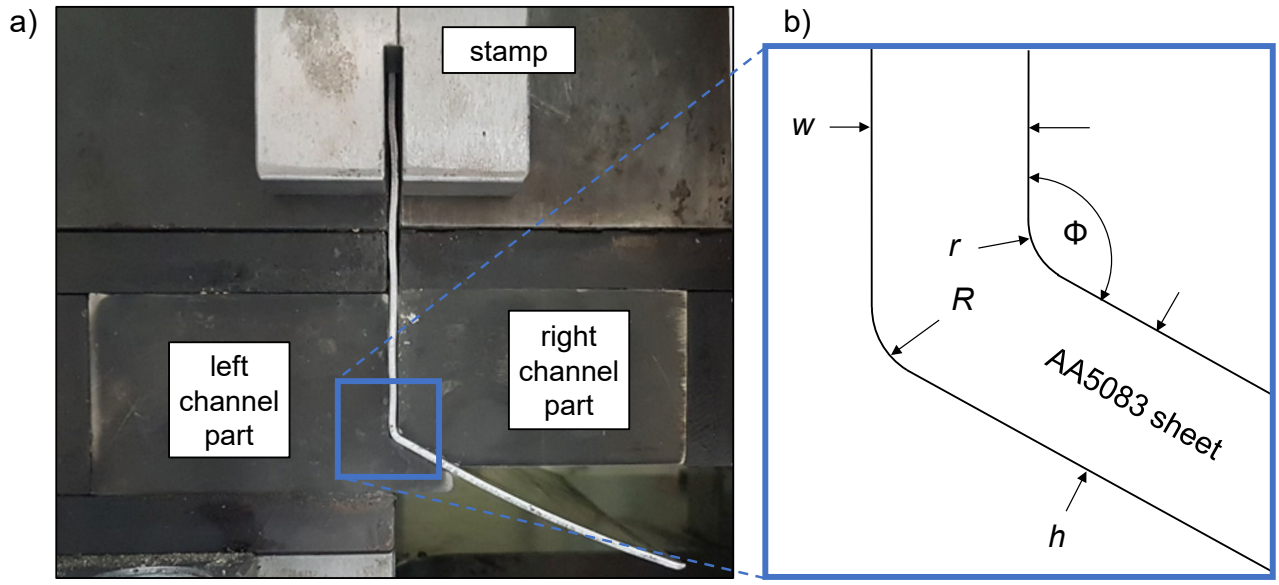

Figure 1: a) ECAP tool for sheet metal with a thickness of 1.8 mm; b) Schematic sketch of the channel geometry and parameters

Determination of High Temperature FLCs on the Novel Test Bench

A new concept for hot forming on a BUP1000 sheet metal forming testing machine was worked out with ZwickRoell GmbH & Co. KG (Germany) in order to test the hot forming capability of the aluminum alloy AA5083 and the ECAP processed sheets under various stress states. Figure 2a) shows the new furnace test bench for a high-temperature test with steel. In principle, the test setup is a Nakajima test with heated dies. Therefore, the process and tool design is based on DIN ISO 12004-2 and the tool consists of a blank holder, a die, and a punch [15]. The test sequence started with the heating of the tool without the sheet to be tested. During heating, the punch lay on a collar in the blank holder and the die lay directly on the blank holder, see Figure 2b). The tool was guided into the furnace on rails. The temperature could be monitored via thermocouples which were in contact with the tool in the furnace. When the tool was at target temperature it was pulled out of the furnace and the die was lifted. The specimen was placed on the hot blank holder and the hot die was in turn placed on the sheet metal specimen. The sheet was then pushed into the furnace again in the closed tool and the heating time, t_1, followed. Then the hot die with the heated specimen was pulled over the rails into the sheet metal testing machine and tested. The sheets have a slight curvature after the ECAP process. However, since the specimens are clamped with a sheet holder force of 400 kN, the specimens can be tested in a flat starting condition. In the present study a stamping speed of 1.5 mm/s was chosen. The tool was designed to be large to store as much heat as possible with the tool mass; the hemispherical punch, for example, has a radius of 50 mm. In this way the temperature loss during the test time, t_2, can be kept low. Digital Image Correlation (DIC) was used to measure the strains during the test. For this purpose the specimens were primed white with boron nitride spray (Henze HeBoCoat SL-E 125) and a stochastic pattern was applied with a black heat-resistant paint (Mipatherm spray). Two layers of graphite foil (the thickness of one layer is 0.7 mm) and boron nitride were used to reduce friction between the stamp and the specimen [3]. To reduce the heat shimmer on the sheet surface, the air was moved through a small computer fan.

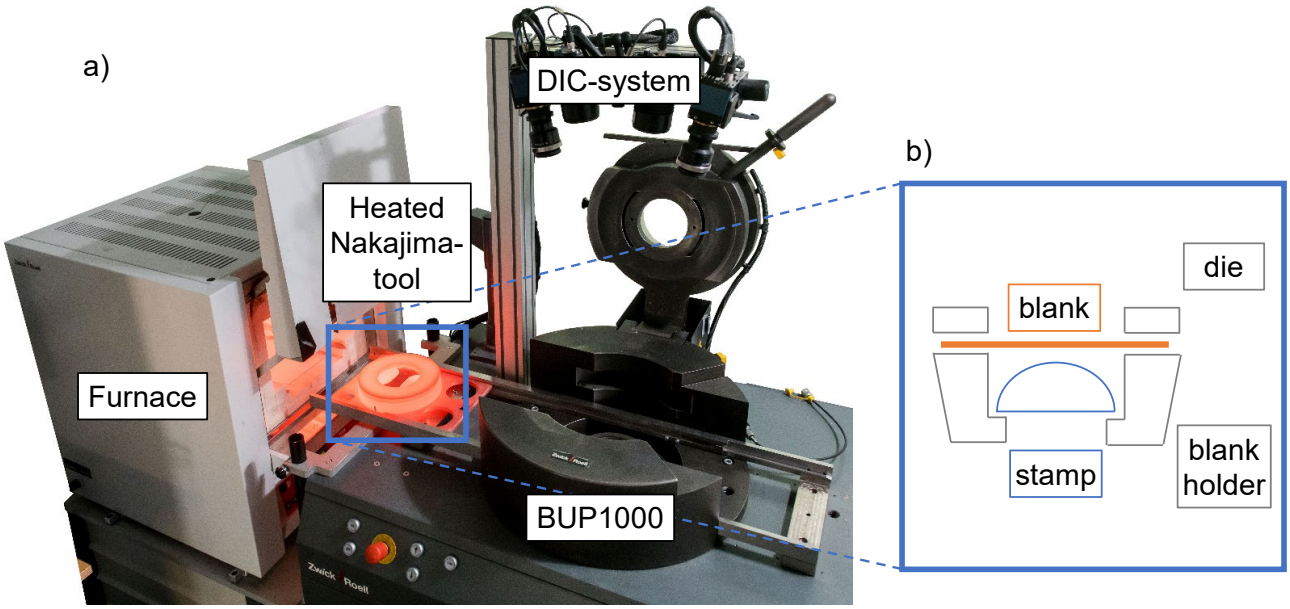

Figure 2: a) Furnace test bench for high temperature forming on a BUP1000 sheet metal forming testing machine using the example of a test with a steel specimen; b) Schematic sketch of the heated Nakajima tool

The tests were carried out with the specimen geometry shown in Figure 3. For the reference material five geometries with different specimen widths were used: 30, 50, 90, 105, 200 mm. For the ECAP material the samples were taken in ED and four geometries were used: 30, 50, 105 and 200 mm.

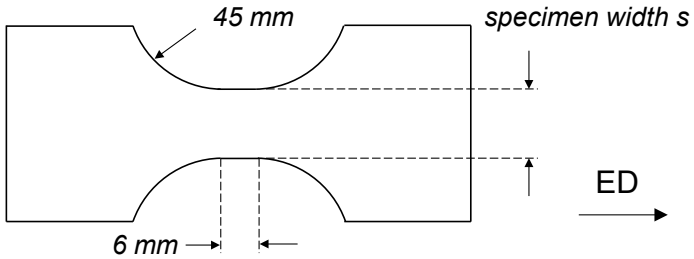

Figure 3: Specimen geometries for the FLC tests

In a previous study on the ECAP material state of the same alloy, a recrystallization temperature of 310 °C was determined by DSC measurements (route C, four passes, equivalent plastic strain per pass ~1.15) [16]. Although higher plastic deformations were present in these investigations and the shear was performed in a different sheet plane, the measured temperature value is used as a reference value since the same material of the same batch was also used in this paper. Since the tool releases heat to the testing machine during the test, and thus the specimen also loses temperature, the specimens are tested in temperature ranges. Thus it is important to set a higher temperature in the specimen during heating, but not exceed the recrystallization temperature of 310 °C for testing without recrystallization effects. The investigations were carried out for the target temperatures of 250 °C and 375 °C to take into account the aspect of recrystallization. The target temperature was defined as the lowest temperature of the tested temperature range, i.e., it was present at the fracture at the end of the test. A pyrometer was used to measure the temperature during the test (CT-SF22-C3, Micro-Epsilon Messtechnik GmbH & Co. KG, Germany). The emission coefficient of the painted sample was calibrated iteratively by comparing temperature values with those obtained from welded-on thermocouples at a distance of 200 mm, resulting in a value of $\varepsilon = 0.96$ for the present configuration (the spectral range of the pyrometer is 8 - 14 µm) [17]. Preliminary investigations showed that the samples are deformed by about 40 mm on average. Therefore the pyrometer was positioned at a

distance of 220 mm from the undeformed initial plane of the sheet. This allowed the most accurate temperature measurement possible throughout the test. To meet the boundary conditions (greater or less than 310 °C), the heating parameters given in Table 1 were used. Figure 4 shows exemplary cooling curves for the specimen geometries 30 and 200 mm. It can be seen that the temperature in the center of the specimen decreased by about 10 % during the test. Nevertheless, the target temperature of 250 °C could be reached without heating the material to above 310 °C. The cooling behavior varied slightly due to the different masses and the contact surface to the tool of the various specimen geometries. Nevertheless, the results of the different specimen geometries were within a range of ± 5 % of the target temperature for the same parameter setup.

Table 1: Heating parameters for the high temperature FLC tests

Target temperature [°C]	Furnace temperature [°C]	Heating time t_1 [s]
250	350	300
375	510	300

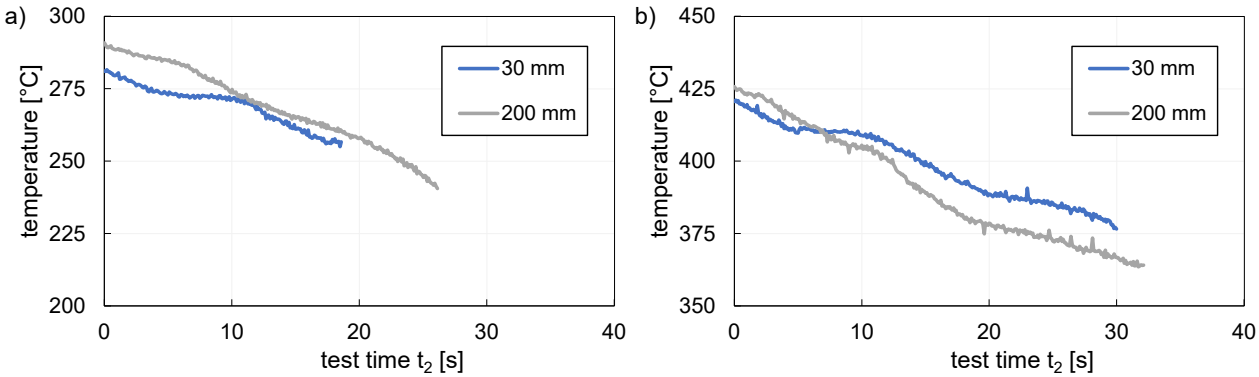

Figure 4: Measured temperature of 30 mm and 200 mm specimens during the test for a) a target fracture temperature of 250 °C and b) 375 °C

The strain measurement was carried out with an Aramis 4M DIC system from GOM mbH (Germany) with a camera resolution of 2400 x 1728 pixels (px). For the investigations at room temperature, the location-dependent cut line method according to DIN EN ISO 12004-2 as implemented in the Aramis software (Aramis professional 2019) was used [15]. To calculate the strains, Aramis uses facets that overlap (point distance). The values und parameters used are shown in Table 2. Due to the higher strains in the temperature-controlled tests, the paint in the pole area sometimes flaked off, making evaluation with the optical measuring system more difficult. To be able to evaluate the crack area reliably, an adjustment of the parameters was proven to be useful, see Table 2. In this case, the interpolation size was chosen to be as small as possible, but large enough so that the area in the pole in the last image before the crack could be resolved. The interpolation size describes the maximum number of adjacent facets that can be interpolated. Despite the integrated fan, there is still a slight heat shimmer on the sheet surface, which is most pronounced in the biaxial specimen (200 mm) at 375 °C. This leads to a scattering of the strains and an average noise floor of the equivalent plastic strain of ~0.0025 (maximum 0.007) can be detected (table 2, “Noise floor of plastic strain”). This is negligible compared to the measured strains in the biaxial range. Standard methods of the Aramis software were used as calculation methods and are also given in Table 2. For the high temperature tests, the Aramis settings had to be adjusted due to the high strains and the slight heat shimmer. This sometimes has an influence on the accuracy of the high temperature results. For the room temperature tests, these expert settings are not necessary and the default settings of the Aramis software are used due to the better accuracy.

In addition, the generation of the best-fit parabola implemented in Aramis often resulted in errors at the elevated temperatures. While data recorded for the specimen widths of 30 mm and 50 mm were usually evaluated correctly by the software, it could be observed that for the samples of widths 90, 105 and 200 mm wrong points were often chosen to generate the parabola. This problem is, for example, also described in [18]. On the one hand, this was due to minimal fluctuations of the measured values caused by the test. As a result, the inner limit values of the points that were still stable and consequently suitable for the best-fit parabola were selected incorrectly. On the other hand, friction caused by the lubrication system at the elevated temperatures was not reduced as much as in the room temperature tests. There is a partial second local maximum due to these friction effects between the sheet and the punch in addition to the crack, see Figure 5. This resulted in an incorrect shape of the best-fit parabola, see Figure 5a). These errors only occured for the major strains of the 90 and 105 mm widths. Both the major and minor strains were affected for the biaxial 200 mm specimens. An alternative evaluation method was developed to counteract these errors, which is based on DIN EN ISO 12004-2 [15]. First, the second derivative of major or minor strain was determined. Then, the inner boundary values to be used for the determination of the best-fit parabola were determined. These points were obtained by searching for the local maximum of the second derivative on both sides of the crack. Only the two closest points were used per crack side unlike as described in DIN EN ISO 12004-2. This had the advantage that in the case of outliers or a second necking, irrelevant points were not included to generate the best-fit parabola. A disadvantage of this method, however, was that it was more unstable and that larger fluctuations and scatter occurred. The best-fit parabola with the form f(x) = ax2 + bx + c was then drawn through the six points determined (orange, dotted curve in Figure 5b). Finally, the maximum of the generated parabola could be calculated. This value represents the stable strain for the corresponding stress state and is approx. 20 % below the measured unstable maximum (grey curve). The corrected evaluation was performed for all specimen geometries and for all cross sections. Subsequent averaging of the maxima yielded the forming limit curve.

Table 2: Aramis parameters for the strain measurement

Parameter	RT	250 °C an 375 °C
Facet size [px]	19	29
Point distance [px]	16	18
Image resolution [px/mm]	~20.2	~18.5
Noise floor of plastic strain [-]	0.0005	0.0025
Interpolation size	0	1 - 6
Calculation method	“More points“	“More points“
Facet matching	start stage	previous stage

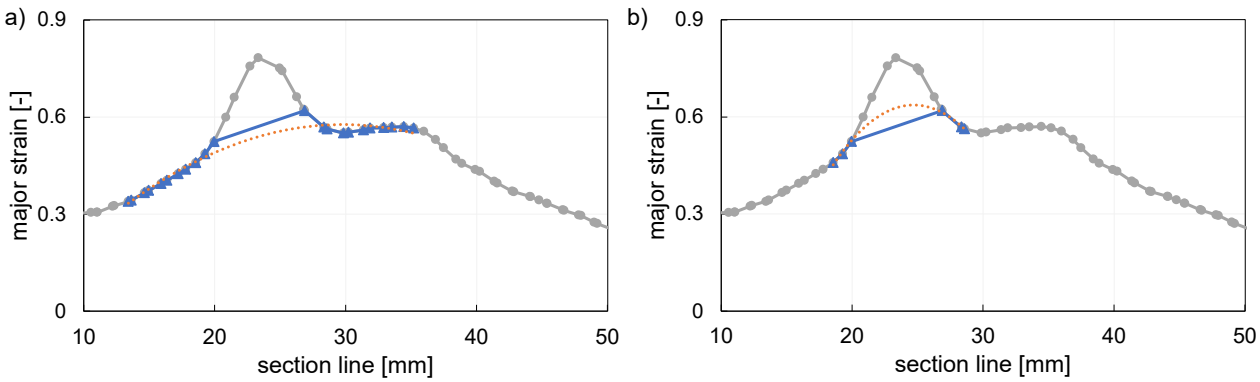

Figure 5: Evaluation of the major strains for a 105 mm specimen with a) the determination by the method of standard DIN EN ISO 12004-2 and b) only six values for determining the best-fit parabola

Due to the decrease in temperature during the test, sensitive deformation mechanisms such as grain boundary sliding during superplastic forming could not be fully investigated. In addition, strain rates of 10^{-2} 1/s were obtained in the tests with a punch speed of 1.5 mm/s. This strain rate tends to be considered be too high for pure superplastic forming. If the test were to be run more slowly, the specimen would cool down even further. Nevertheless, processes close to the industrial applications like Quick Plastic Forming (QPF) can be mapped and material parameters for hot forming can be determined very accurately with the novel test bench [19].

Results and Discussion

Figure 6 shows the Forming Limit Diagram (FLD) of the reference material and the ECAP processed sheet metal for RT, 250 °C and 375 °C. Every data point was determined from tests on at least three specimens. The Nakajima test for the ECAP specimens at room temperature shows that the forming limit curve is significantly lower than in the Nakajima test for the reference material at room temperature. The reasons for this are the dislocations introduced in the microstructure by the ECAP process. Thus, the ductility decreases and the specimen fails earlier [20]. In addition, ECAP results in damage to the material surface. Particularly with regard to the sheet semifinished product, these surface defects have a greater influence than with ECAP of bulk material. In the tests at room temperature, the greatest deformation capacity is found under biaxial strain (200 mm specimen). Thus, principal strains of 0.28 are obtained for the reference material and 0.17 for the ECAP condition. The minima of the FLCs (105 mm) are found between plane strain and biaxial strain.

The strain hardening capacity and the yield strength decrease above temperatures of 100 °C. At the same time, the dynamic debonding process increases due to recrystallization and recovery processes, resulting in an increase in fracture strain and necking [1]. In general, the FLCs shift significantly upward as a result. The deformation capacity of the reference material at 250 °C is increased by about 300 % in the uniaxial range (30 mm) compared to the investigations at room temperature. For the ECAP material, the increase is about 700 %. Moreover, the minima of the FLCs no longer occur in the plane strain region, but in the biaxial stretching region. This is also consistent with the results of Naka et al. and Bressan et al. [21,22]. It can already be seen for this temperature range that the scatter of the test results becomes larger, especially for the ECA-pressed sheets. As mentioned above, this is on the one hand a result of the modified evaluation method. On the other hand, the ECAP sheets still contain slight surface defects which can also lead to deviations in the failure range.

Compared with the tests at 250 °C, it can be seen that the FLCs for 375 °C are shifted upwards again and the forming capacity increases. The curves of the reference material and the ECAP specimens are now superimposed. In the uniaxial range, the ECAP specimens exhibit even higher strains than the reference material. The larger scatter of the ECAP material can again be explained by the damaged sheet surface and the evaluation procedure. Nevertheless, the values are within an acceptable range for these high strains. The largest increase occurs in the uniaxial region with specimen width of 30 mm. This may indicate that the different microstructural deformation mechanisms have different degrees of influence, depending on the stress state. For example, the grains can slide well against each other in the uniaxial tension region. Based on the strain rate and temperature used in this series of experiments, it can be concluded that we are at the limit of the range where superplasticity can in principle occur. To take full advantage of this mechanism, strain rates would likely need to be smaller ($<10^{-3}$ 1/s) and the temperature more constant [3,23].

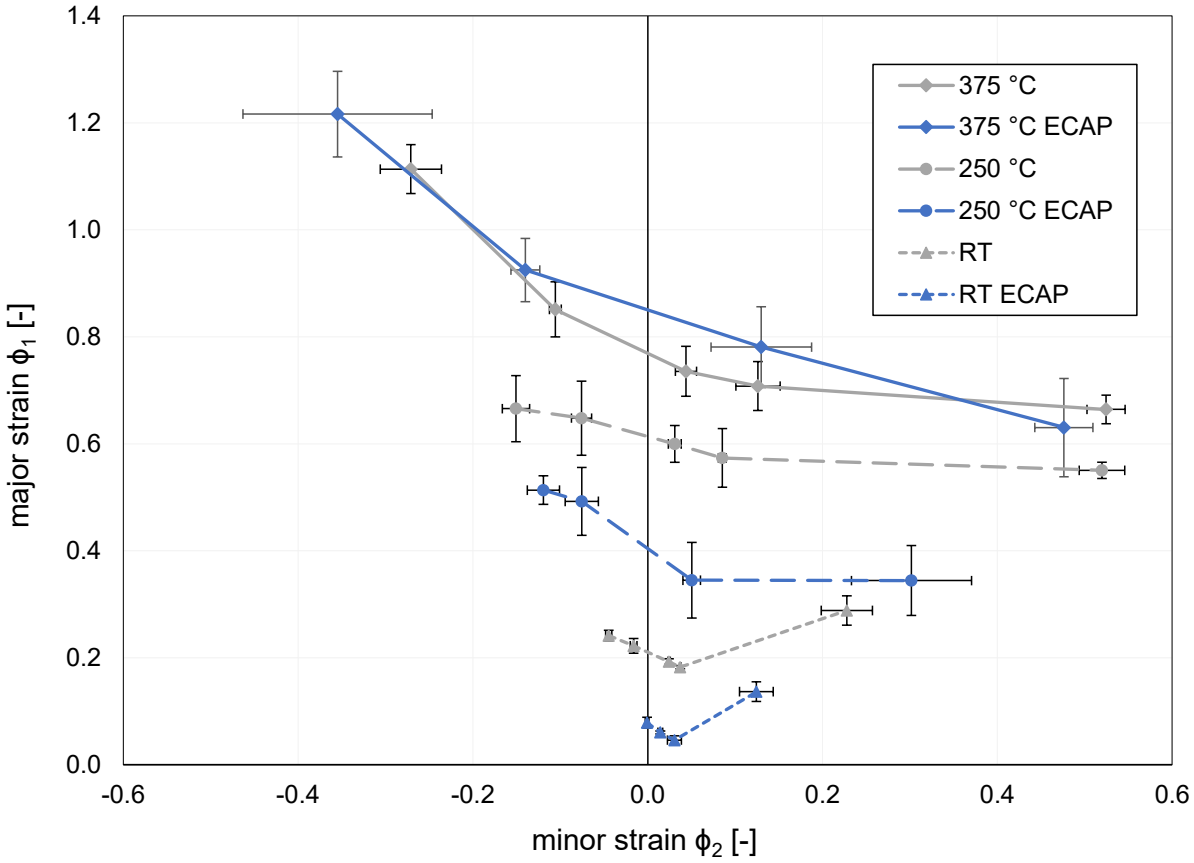

Figure 6: Forming limit diagram of the reference material and the ECAP processed sheet metal for RT, 250 °C and 375 °C

Figure 7 shows the forces versus displacement of the stamp for the specimens with widths of 30 and 200 mm at the three temperatures studied. Representative data from individual specimens instead of mean values are shown in the plots. At room temperature, the ECA-pressed specimens can be deformed far less (see also FLC in Figure 6), but for the same displacement the forming force increases more steeply (see Figure 7a). The steeper force signal results from the increase in yield strength due to the ECAP process. However, since the ECAP sample fails early, the maximum at RT for the reference material is higher for the 200 mm sample. A stronger increase in force of the ECAP specimens is also seen for forming at 250 °C (Figure 7b). Here, the curve maxima are now above those of the reference material. Thus, higher strengths and stiffnesses are also present at this forming temperature, and more force is required to deform the material. The effect is even more pronounced at a forming temperature of 375 °C, see Figure 7c). These results illustrate the potential of ECAP sheets: They can be formed at elevated temperatures to similar strains as the reference material. Moreover, due to its higher resistance to deformation, the ECAP material offers great lightweight potential, especially in applications such as body construction in the automotive industry.

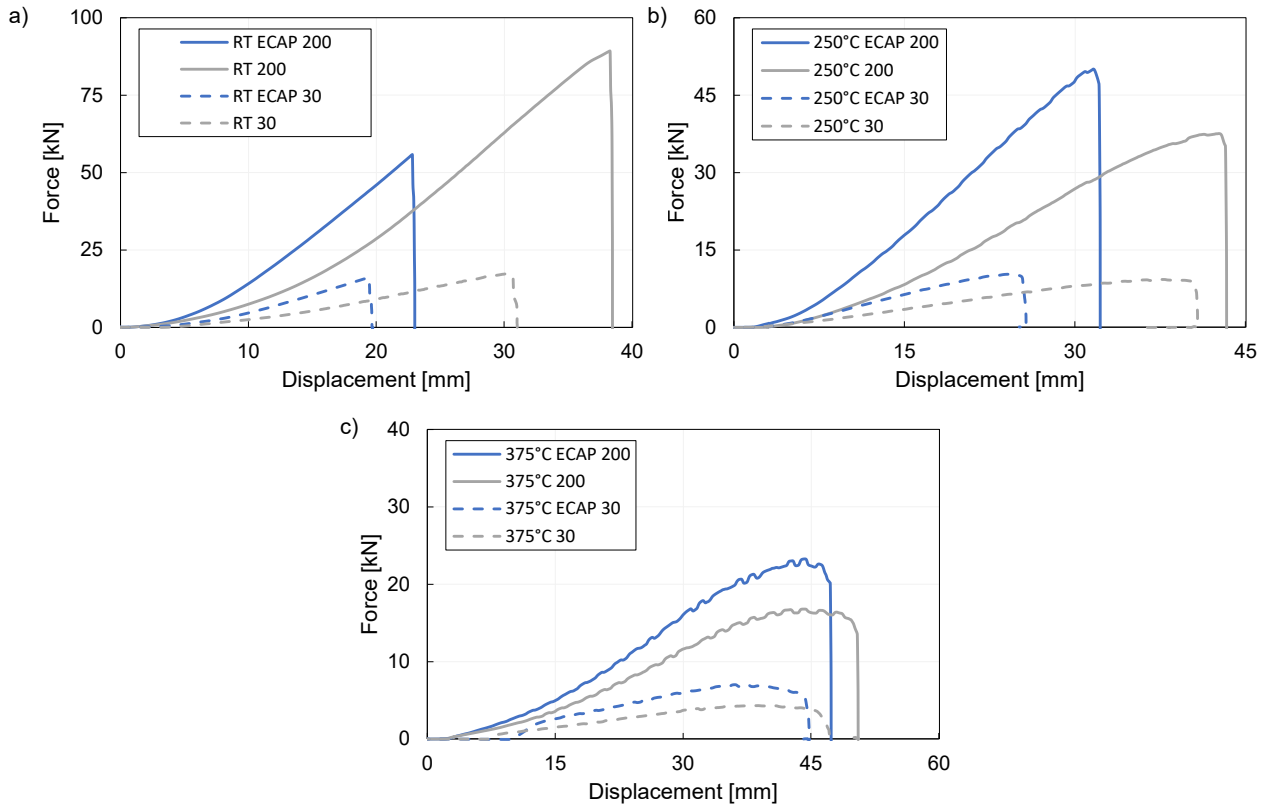

Figure 7: Force – Displacement curves for specimens with 30 mm (dashed lines) and 200 mm (solid lines) geometries of the reference (grey) and the ECAP (blue) material at a) RT, b)250 °C and c) 375 °C

Finally, in order to obtain further insights into deformation and failure mechanisms, optical microscopy was performed on the fracture surfaces. Figures 8a) – c) show the fracture surfaces of exemplary 30 mm and 200 mm specimens at 50x magnification. At room temperature, local necking can be observed in the reference material in the uniaxial state (30 mm specimen). In the biaxial case (200 mm specimen), more global necking can be observed, and under both stress conditions the material exhibits brittle failure. In the ECAP specimens, no necking is observed under both stress states (uniaxial and biaxial) and the specimens fail entirely by brittle shear fracture. As expected, the deformation behaviour is thus strongly influenced by SPD processing.

The uniaxially deformed reference specimens tested at 250 °C exhibit elongated plastic zones, which are typical of a mixture of conventional dislocation motion and diffusive processes (diffusion creep) [23]. The accompanying increase in necking and fracture strain changes from shear fracture, which is typical at low temperatures, to necking fracture [1]. The uniaxial ECAP specimens (30 mm) show much less necking at this temperature. For the biaxial ECAP specimens (200 mm), there is no local but only global necking.

At 375 °C, in the uniaxial case, the reference material undergoes a more pronounced localized necking than the ECAP material, see Figure 8c). The large plastic strain and increased necking in the reference material results in elongated cavities, which are nucleated predominantly at precipitates (Figure 8d, blue frame, black arrows). The cavities merge along the tensile axis to form thin, strip-like structures. This type of cavity formation was recognized by Kulas et al. as indicative of predominant solute drag creep as a deformation mechanism [24]. However, for the ECAP material (Figure 8d, grey frame), larger cavities sometimes open in the material and not conspicuous close to precipitates. This may be related to the lower material flow from the sheet thickness. Grain boundary sliding now likely also contributes to this type of cavity formation. In general, grain boundary sliding and diffusion creep act together at the selected strain rate and temperature range. While, again, slower strain rates and more

constant temperatures would be needed to facilitate superplastic forming, the potential for QPF is evident from these observations [23]. If the ECAP process for sheet materials can also be further improved in such a way that the surface is damaged even less, there is additional potential for further improvement. An example for potentially beneficial improvements of sheet metal ECAP is the superposition of a backpressure, which is to be worked out in future work.

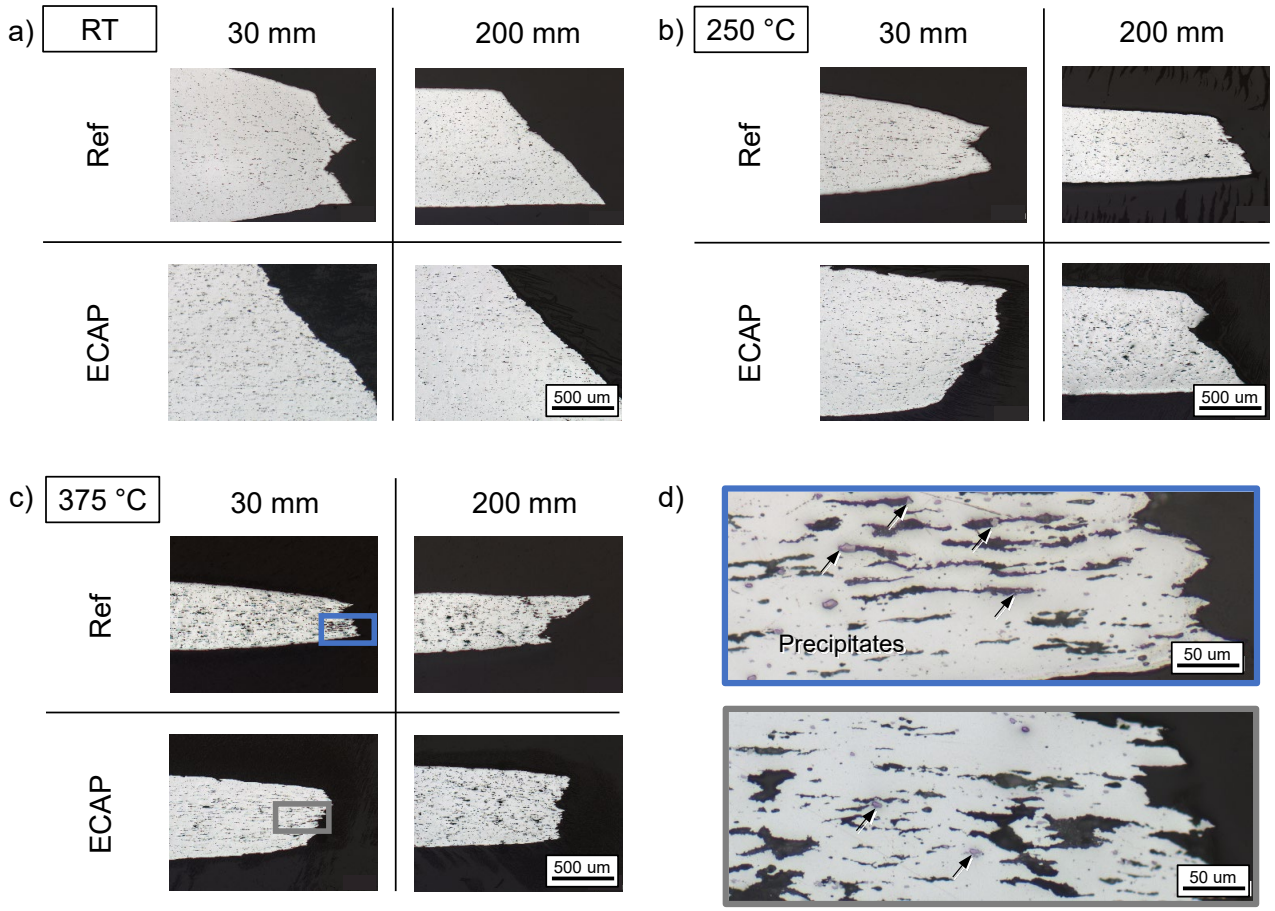

Figure 8: Optical micrographs of the deformed specimens at a) RT, b) 250 °C and c) 375 °C; d) 500x magnification of the reference (blue frame) and ECAP (grey frame) material of the 30 mm specimen deformed at 375 °C

Conclusion and Outlook

In this study, a high temperature forming furnace test bench for the determination of FLCs was set up and put into operation. In order to demonstrate the forming behavior of aluminum sheet materials during hot forming, forming limit curves of an AA5083 alloy were tested at room temperature, 250 °C and 375 °C. In addition, the material was processed using an ECAP method for sheet materials. The forming limit curves, and the force-displacement diagrams, show the lightweight potential due to ECA-pressing. The following key findings were obtained:

- The ZwickRoell furnace test bench offers the possibility of recording forming limit curves at elevated temperatures in a BUP1000 sheet metal forming testing machine. Here, the drop in temperature during the test (approx. 10 % of the initial heating temperature) must be considered, so as not to test in temperature ranges in which microstructural transformations or similar occur. For high test temperatures, this can be counteracted by a higher heating temperature.
- Above the recrystallization temperature (tests at 375 °C), similar deformations to the reference specimens are obtained for the ECAP-processed specimens in plane and biaxial strain. For the uniaxial stress state, higher strains can be obtained for the ECAP specimens.

- Optical microscopy of fracture regions indicates that, at the temperatures above the recrystallization temperature for the ECAP material, the deformation mechanism of grain boundary sliding acts alongside diffusion creep processes. We note in closing that, to investigate the potential of the ECAP material for superplastic forming in more detail, constant temperature tensile tests at lower strain rates would be even more appropriate to further demonstrate the potential for Quick Plastic Forming and lightweight construction.

Acknowledgements

The authors gratefully acknowledge funding by the German Research Foundation (Deutsche Forschungsgemeinschaft, DFG) in supporting this work within the framework of the collaborative research projects VO 1487/32-2 and WA 2602/13-2. Thank you to Corinna Sutter who helped to prepare the microscopic specimen. The authors would also like to thank the ZwickRoell GmbH & Co. KG for the cooperation on the furnace test bench. On behalf of all project participants, Ralf Schierloh, Manfred Rattunde, Harald Maier, Fritz Gerster and Manuele Campus should be mentioned here in particular.

References

[1] F. Ostermann, Anwendungstechnologie Aluminium, Berlin, Heidelberg: Springer Berlin Heidelberg, 2014.

[2] H. Ribes, Aluminum Applications in Lightweight Design for Small Commercial Vehicles and Station Wagons, ATZprod worldwide, 2019, no. 6:42–45.

[3] P.F. Bariani, S. Bruschi, A. Ghiotti, and F. Michieletto, Hot stamping of AA5083 aluminium alloy sheets, CIRP Annals, 62 (2013), 251–254.

[4] R. Neugebauer, T. Altan, M. Geiger, M. Kleiner, and A. Sterzing, Sheet metal forming at elevated temperatures, CIRP Annals, 55 (2006), 793–816.

[5] K. Siegert, Blechumformung, Berlin, Heidelberg: Springer Berlin Heidelberg, 2015.

[6] T.G. Langdon, The mechanical properties of superplastic materials, Metallurgical Transactions A, 13A (1982), 689–701.

[7] F. Klocke, and W. König, Fertigungsverfahren 4: Umformen, SpringerLink Bücher, Berlin, Heidelberg: Springer Berlin Heidelberg, 2006.

[8] M. Kawasaki, and T.G. Langdon, Principles of superplasticity in ultrafine-grained materials, Journal of Materials Science, 42 (2007), 1782–1796.

[9] M.F.-X. Wagner, N. Nostitz, S. Frint, P. Frint, and J. Ihlemann, Plastic flow during equal-channel angular pressing with arbitrary tool angles, International Journal of Plasticity, 134 (2020).

[10] J. Suh, J. Victoria-Hernandez, D. Letzig, R. Golle, S. Yi, J. Bohlen, and W. Volk, Improvement of Ductility at Room Temperature of Mg-3Al-1Zn Alloy Sheets Processed by Equal Channel Angular Pressing, Procedia Engineering, 81 (2014), 1517–1522.

[11] M. Gruber, C. Illgen, P. Frint, M.F.-X. Wagner, and W. Volk, Numerical and Experimental Study on ECAP-Processing Parameters for Efficient Grain Refinement of AA5083 Sheet Metal, Key Engineering Materials, 794 (2019), 315–323.

[12] P. Frint, M.F.-X. Wagner, S. Weber, S. Seipp, S. Frint, and T. Lampke, An experimental study on optimum lubrication for large-scale severe plastic deformation of aluminum-based alloys, Journal of Materials Processing Technology, 239 (2017), 222–229.

[13] M. Gruber, Y. Yang, C. Illgen, P. Frint, M.F.-X. Wagner, and W. Volk, Thermomechanical Analysis and Experimental Validation of ECAP for Aluminum Sheet Metal, Forming the Future, ed. G. Daehn et al., The Minerals, Metals & Materials Series, vol. 1, Cham: Springer International Publishing, 2021, 1775–1790.

[14] Y. Iwahashi, J. Wang, Z. Horita, M. Nemoto, and T.G. Langdon, Principle of Equal-Channel Angular Pressing for the Processing of Ultra-Fine Grained Materials, Scripta Materialia, 35 (1996), 143–146.

[15] DIN EN ISO 12004-2, Metallische Werkstoffe – Bleche und Bänder - Bestimmung der Grenzformänderungskurve: Teil 2: Bestimmung von Grenzformänderungskurven im Labor, DIN Deutsches Institut für Normung e.V., 34 pp., 2008.

[16] C. Illgen, B. Bohne, M.F.-X. Wagner, M. Gruber, W. Volk, and P. Frint, Facing the Issues of Sheet Metal Equal-Channel Angular Pressing: A Modified Approach Using Stacks to Produce Ultrafine-Grained High Ductility AA5083 Sheets, Advanced Engineering Materials, 1 (2021), 2100244.

[17] K.W. Gerhardt, Untersuchungen zur konduktiven Erwärmung für Warmzugversuche an Blechen, Dissertation, Shaker Verlag GmbH, 2015.

[18] W. Hotz, M. Merklein, A. Kuppert, H. Friebe, and M. Klein, Time Dependent FLC Determination Comparison of Different Algorithms to Detect the Onset of Unstable Necking before Fracture, Key Engineering Materials, 549 (2013), 397–404.

[19] M.-A. Kulas, P.W. Green, E.M. Taleff, P.E. Krajewski, and T.R. McNelly, Deformation Mechanisms in Superplastic AA5083 Materials, Metallurgical and Materials Transactions A, 2005, 36A:1249–1261.

[20] R.Z. Valiev, I.V. Alexandrov, Y.T. Zhu, and T.C. Lowe, Paradox of strength and ductility in metals processed by severe plastic deformation, Journal of Materials Research, 17 (2002), 5–8.

[21] T. Naka, G. Torikai, R. Hino, and F. Yoshida, The effects of temperature and forming speed on the forming limit doagram for type 5083 aluminum-magnesium alloy sheet, Journal of Materials Processing Technology, 113 (2001), 648–653.

[22] J.D. Bressan, L.P. Moreira, M.C. dos Santos Freitas, S. Bruschi, A. Ghiotti, and F. Michieletto, Modelling of Forming Limit Strains of AA5083 Aluminium Sheets at Room and High Temperatures, Advanced Materials Research, 1135 (2016), 202–217.

[23] S. Bruschi, A. Ghiotti, and F. Michieletto, Hot Tensile Behavior of Superplastic and Commercial AA5083 Sheets at High Temperature and Strain Rate, Key Engineering Materials, 554-557 (2013), 63–70.

[24] M.-A. Kulas, P.W. Green, E.M. Taleff, P.E. Krajewski, and T.R. McNelly, Failure mechanisms in superplastic AA5083 materials, Metallurgical and Materials Transactions A, 37 (2006), 645–655.